2017 International Conference on Alternative Energy in Developing Countries and Emerging Economies, 2017 AEDCEE, 25-26 May 2017, Bangkok, Thailand

Improving global accessibility to offshore wind power through decreased operations and maintenance costs: a hydrodynamic analysis

Ariel J. Edesess[1,*], Denis Kelliher[1], Alistair G. L. Borthwick[2], Gareth Thomas[3]

Abstract

Improved access to renewable energy in developing economies will be a major factor in future global efforts to reduce CO_2 emissions, while simultaneously raising living conditions in areas presently without or with only limited access to electricity. Coastal populations stand to benefit greatly from reduced costs of offshore wind farms, which are one of the fastest growing and most economical sources of marine renewable energy. A considerable drawback of offshore wind power is the high cost of operations and maintenance (O&M), which can account for 25-50% of total energy production costs. Present-day maintenance procedures, using crew transfer vessels, rely on the significant wave height (H_S) as the limiting factor by which to decide whether or not it is safe to access the offshore turbines. In practice, H_S has to be applied conservatively, thus raising the costs through increased downtime. A method is proposed here with the objective of reducing overall costs through improved analysis of the motion of the crew transfer vessels (CTVs) used to transport repair technicians onto offshore wind turbine structures. CTV motion depends on the hydrodynamic forces incident on the vessel under operating conditions and the effect that the presence of the turbine has on the flow field. A change in the hydrodynamic field caused by the turbine monopile can cause a vessel abutted against the turbine support column to lose frictional contact and slip. Using the open-source computational fluid dynamics software, OpenFOAM, and *in situ* experimental results, the diffracted surface elevation and a wave kinematics model for the near-wake of a turbine monopile are presented. More accurate estimates of significant wave height and wave kinematics incident on a vessel close to a turbine monopile will facilitate much improved analysis of vessel motions under operational conditions.

1. Introduction

Efforts to reduce CO_2 in the Earth's atmosphere has resulted in a global shift from energy produced by large-scale coal and gas (CCGT) power plants to energy produced from renewable sources. Although

*a.edesess@umail.ucc.ie
[1]The Department of Civil and Environmental Engineering, University College Cork, Cork, Ireland
[2]School of Engineering, The University of Edinburgh, Edinburgh, EH9 3JL, United Kingdom
[3]Department of Applied Mathematics, University College Cork, Cork, Ireland

such efforts have been mainly concentrated in the developed world, as of June 2016, 174 countries had adopted some form of renewable energy target [1]. In 2015, global investment in renewable energy in emerging economies surpassed the corresponding investments in more industrialised countries [2]. For coastal populations that have an average density that is nearly three times that of the average global density [3], the marine environment provides a promising portfolio of renewable energy sources. Of these, offshore wind power is the fastest growing and most economical source for marine renewable energy.

In 2015, an estimated 3.4 GW from offshore wind power was connected to the grid, leading to a global total of 12 GW, of which 91% is in Europe and the remaining 9% is mostly located in China, Japan, and South Korea [4]. At the beginning of 2016, the European grid had more than 3,000 offshore wind turbines connected to it [5]. Outside Europe, China set the ambitious goal of 30 GW of offshore wind energy by 2020 [6]. However, due to a lack of marine spatial planning and increasing costs, only 1 GW out of the target of 5 GW has been installed to date [6]. India has also introduced and approved policies to initiate offshore wind power, but does not yet have any installed capacity. For coastal populations, the majority of whom live in Asia, increased development of offshore wind farms provides considerable potential for the production of clean energy, countering the present situation where access to electricity is often insufficient, unsustainable, or produces harmful pollutants. Noting that estimates vary widely, offshore wind power nevertheless has huge potential especially for densely populated coastal hubs in developing countries: Krewitt *et al.* [7] have assessed the technical potential to be about 16,000 $(TW.h).a^{-1}$ by 2050 and Capps & Zender [8] calculated the overall global value of offshore wind energy to be approximately 340,000 $(Tw.h)a^{-1}$.

A substantial portion of the total monetary investment is put into O&M, which can account for 25-50% of total energy production costs [9, 10]. O&M costs mainly arise from the hiring of repair workers and transport vessels. Rushed efforts to develop offshore wind farms to help meet global emissions targets have resulted in an absence of regulations concerning the best methods to access turbines for maintenance, potentially leading to unfinished repairs or danger to the repair technicians [11, 12, 10]. Small CTVs, which can be monohulls, catamarans, or SWATH type vessels, account for 46% of turbine access methods [9]. However, CTVs are limited by weather and sea state conditions and are typically only available when $H_s < 1.5\ m$, where H_s is the significant wave height [9, 13]. Throughout crew transfer to the monopile, the CTV is driven directly into the monopile's transition piece and, using a steady thrust from the engine, contact between the CTV and the turbine is maintained solely through frictional forces [10]. The transition piece or boat landing is located downstream of the turbine, depending on the prominent wave direction at that location (see Figure 1).

Whilst the CTV is abutted against the turbine, the presence of the turbine may alter the passing wave field and potentially affect CTV motion. To understand the water particle kinematics in the vicinity of the turbine and later vessel motion, the model problem is introduced as the flow around a cylinder, where the turbine is simplified as a smooth surface-piercing bottom-fixed cylinder. The aim of the study is to determine the influence of the monopile on the wave

Fig. 1: Simplified CTV and Monopile System

field. In the following sections, numerical and analytical methods are presented by which to calculate the surface elevation and water particle kinematics in the vicinity of the turbine and compute the forces incident on the turbine for varying wave periods.

2. Governing Equations

Flow past a cylinder is considered to be a classic problem in fluid dynamics; Sarpkaya & Isaacson [14], Zdravkovich [15], and Sumer & Fredsøe [16] all provide in-depth reviews. For small diameter cylinders that do not alter the pressure field in the flow, the Morison Equation is commonly used to calculate the combined transient drag and inertial forces acting on the cylinder; from Sarpkaya & Isaacson [14] this is
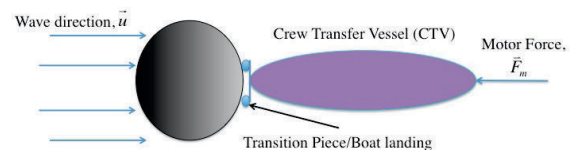
$$\mathbf{F_T} = \rho C_m \frac{\pi D^2}{4} \int_{z=-h}^{z=\eta} \dot{\mathbf{u}}(x,z,t)dz + \frac{1}{2} C_d D \rho \int_{z=-h}^{z=\eta} |\mathbf{u}(x,z,t)| \mathbf{u}(x,z,t)dz, \tag{1}$$

where ρ is the fluid density, D is the cylinder diameter, $\mathbf{u}(x,z,t)$ is the incident velocity vector, $\dot{\mathbf{u}}(x,z,t)$ is the incident water particle acceleration vector, and C_d and C_m are the drag and inertia coefficients respectively. The values of C_d and C_m are dependent upon the non-dimensional Reynolds number ($Re = \frac{U_\infty D}{\nu}$) and Keulegan-Carpenter number ($KC = \frac{T U_\infty}{D}$), where ν is the coefficient of fluid kinematic viscosity, U_∞ is the incident velocity magnitude and T is the wave period (see e.g. [17]). When Re is high ($Re > 1x10^6$) and KC is low ($KC < 1$), a third parameter, $\beta = Re/KC$, is introduced which can be used to calculate the drag and inertial coefficients using the formulation introduced by Wang [18]. From Wang's theory, C_d and C_m are given by

$$C_a = 1 + 4(\pi\beta)^{-1/2} + (\pi\beta)^{-3/2} \tag{2}$$

and

$$C_d = \frac{3\pi^3}{2KC} \left[(\pi\beta)^{-1/2} + (\pi\beta)^{-1} - \frac{1}{4}(\pi\beta)^{3/2} \right], \tag{3}$$

where C_a is the added mass coefficient and is related to the inertial coefficient by $C_m = 1 + C_a$. Integrating over the depth from $-h < z < \eta$, where h is the water depth and η is the location of the free surface above mean water, gives the total transient forces over the length of the cylinder. For large diameter cylinders (i.e. where $D/L > 0.2$), inertia forces dominate and the presence of the cylinder changes the surrounding pressure field thereby producing a diffraction force [17]. An analytical solution introduced by MacCamy & Fuchs [19] exists for the calculation of the combined diffracted and incident forces and should be equivalent to the inertial term in equation (1). The incident force is called the Froude-Krylov force and is produced by the unsteady pressure field created by the undisturbed waves. The Froude-Krylov force is dependent only on the density ρ, the monopile diameter D and the fluid accleration $\dot{\mathbf{u}}$. Combing the incident force with a solution for the diffraction force gives the total non-viscous forces acting on the monopile. The inertial dominant force incident on the monopile is given by

$$\mathbf{F_T} = \frac{2\rho g H}{k} \int_{z=-h}^{z=\eta} \frac{\cosh k(h+z)}{\cosh kh} G\left(\frac{D}{L}\right) \cos(\omega t - \psi)\, dz \tag{4}$$

where

$$\tan\psi = \frac{J_1'(ka)}{Y_1'(ka)} \quad \text{and} \quad G\left(\frac{D}{L}\right) = \frac{1}{\sqrt{J_1'(ka)^2 + Y_1'(ka)^2}} \tag{5}$$

and J_m is a Bessel function of the first kind, Y_m is a Bessel function of the second kind and the prime denotes a derivative with respect to the quantity in brackets [19, 20]. Similarly, the surface elevation can be given as a combination of the incident and diffracted components

$$\eta(x,y,t)_{diff} = a\cos m\theta \sum_{m=1}^{\infty} \varepsilon_m (i)^{-m} \left(J_m(kR) - H_m^{(2)}(kR) \frac{J_m'(kR)}{H_m^{(2)'}(kR)} \right) \cos\omega t \tag{6}$$

where $H_m^{(2)}$ is a Hankel function of the second kind, a is the wave amplitude, θ is the angular location around the cylinder circumference, and ε equals 1 when $m = 0$, and 2 otherwise. Comparing the form of equation (4) to the inertia term in equation (1) shows the significance of diffraction effects on the total force. A second comparison can be made between the diffracted surface elevation η_{diff} in eqn. (6), the simulated surface elevation η_{OF} and the analytical undisturbed incident wave field, $\eta(x,t)_\infty = a\cos\omega t$.

3. Numerical Procedure

The open-source C++ library of fluid solvers, OpenFOAM, is used to simulate free surface waves around a cylinder in a channel; this uses a modified version of the multiphase solver *interFoam* called *waveFoam*, developed by Jacobsen *et al.* [21]. It can be assumed that only small-amplitude linear waves are applicable due to the H_s limits for the CTV (see Section 1). Relaxation zones of length L, where L is the wavelength, are placed at the inlet and outlet of the computational domain to act as absorbing layers for the outgoing and reflected waves. The computational domain has a total length of $4L$ for $L \geq 10D$ and $6L$ for $L < 10D$. A minimum of 75 cells per wavelength was used in the horizontal direction and 7 cells per wave height in the vertical direction. More details of the numerical implementation are provided in Edesess *et al.* [22]. Wave gauges placed throughout the domain are used to interpolate along the z-axis to provide the velocity particle kinematics and the surface elevation, $\eta(x,t)_{OF}$ to measure the effects that the turbine has on the passing fluid flow. Information on the velocity components and diffracted surface elevation are stored, using 16 numerical probes and wave gauges at intervals of $\pi/8$ around the cylinder and towards the inlet of the domain. Comparison between the forces calculated using equations (1) and (4) demonstrates the effect of the monopile turbine on the incident pressure field and the relative importance that the wave period has on changes to the pressure field.
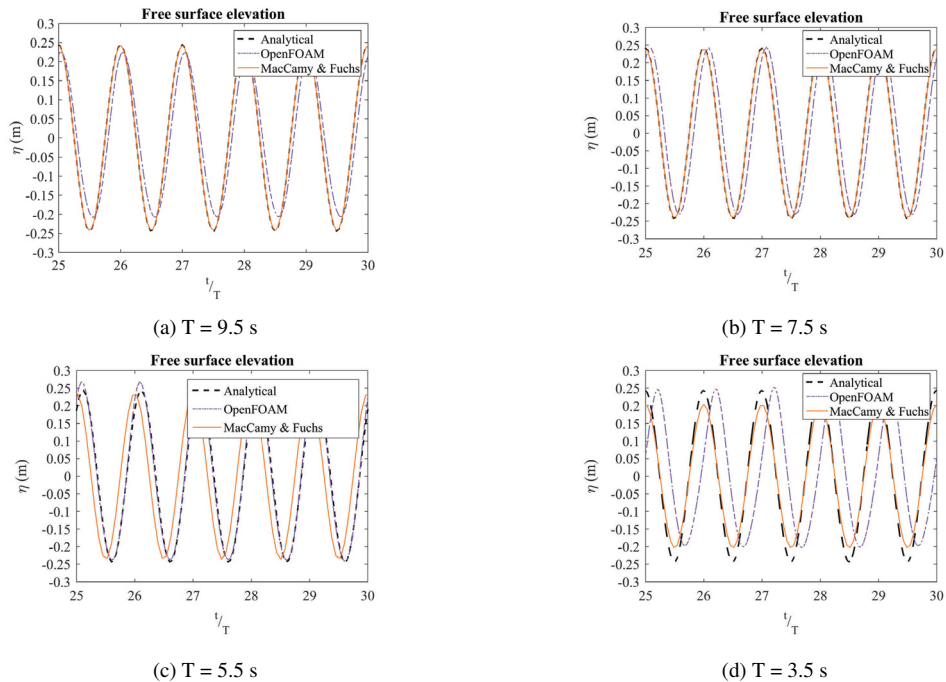
4. Results

Wind farm data were provided by the Operations Team at EDF Energy Renewables Teesside Offshore Wind Farm. Typical turbines at this wind farm have diameter $D \sim 5$ m. Assuming smal- amplitude waves where $a_{max} = H_s/2 \approx 0.75$ m and water depth $h = 15$ m, with velocities $U_\infty < 1$ m/s. Representative wave periods for the geographical area are $T_p \sim 3 - 10$ s, corresponding to wavelengths of $L \sim 20 - 100$ m, or $D/L \sim 0.25 - 0.05$ [10]. The values of T and D/L are given in Table 1. Forces were calculated using the Morison Equation (eqn. 1), the MacCamy & Fuchs diffraction solution (eqn. 4), and through integration of the surface pressure around the monopile. Taking a Fourier transform of the force time series, the power spectral density function (PSD) was calculated to determine the peak power for each method, as listed in Table 1. In Table 1, the subscript "*Mor*" denotes the Morison Equation, "*Mac*" indicates the diffraction method and "*P*" stands for the integrated pressure method.

Surface elevations were compared between the numerically simulated free-surface, the analytical solution for the diffracted free surface (eqn. 6), and the undisturbed linear surface elevation, $\eta = a\cos\omega t$. Figures(2a-2d) show comparisons for four different wave periods. Twenty-five samples per wave cycle were taken from numerical wave gauges placed towards the inlet along the centreline. An additional sixteen wave gauges were placed at intervals of $\pi/8$ around the cylinder to determine the simulated diffracted surface elevation. Table 2 presents values obtained for the drag and inertia coefficients C_D and C_m, respectively, which were calculated using eqns. (2) and (3). The subscript *OF* refers to numerical values and *An* refers to analytical values derived from linear wave theory.

Wave Period	T1	T2	T3	T4
D/L	0.26	0.125	0.07	0.05
Max_{Mor}	2.54×10^{11} N^{2}Hz^{-1}	3.38×10^{11} N^{2}Hz^{-1}	1.11×10^{11} N^{2}Hz^{-1}	6.5×10^{10} N^{2}Hz^{-1}
Max_{MF}	1.69×10^{11} N^{2}Hz^{-1}	3.13×10^{11} N^{2}Hz^{-1}	2.43×10^{11} N^{2}Hz^{-1}	1.64×10^{11} N^{2}Hz^{-1}
Max_{P}	1.48×10^{11} N^{2}Hz^{-1}	3.37×10^{11} N^{2}Hz^{-1}	2.85×10^{11} N^{2}Hz^{-1}	1.96×10^{11} N^{2}Hz^{-1}

Table 1: Total Energy and Peak Values calculated from the PSD of total forces

Table 2 lists results for several parameters, including the non-dimensional drag and inertial coefficients, the Keulegan-Carpenter and β frequency parameter.

(a) T = 9.5 s

(b) T = 7.5 s

(c) T = 5.5 s

(d) T = 3.5 s

Fig. 2: Free surface Elevation η for each wave period

Wave Period	T1	T2	T3	T4
$C_{d,(OF)}$	0.0527	0.0488	0.0494	0.0489
$C_{d,(An)}$	0.0321	0.0395	0.0429	0.0441
$C_{m,(both)}$	2.136	2.158	2.149	2.166
KC_{OF}	0.187	0.243	0.287	0.327
$KC_{An.}$	0.306	0.311	0.331	0.363
$U_{\infty,(OF)}$	0.266	0.221	0.197	0.176
$U_{\infty,(An.)}$	0.438	0.283	0.227	0.197
β	7.14×10^6	4.54×10^6	3.42×10^6	2.69×10^6

Table 2: Non-Dimensional Values

5. Discussion and Conclusions

Linear waves were simulated for the four different wave periods listed in Table 1. The surface elevation in the vicinity of a monopile turbine and the incident force spectrum were calculated using a number of different methods and the predictions compared. The predicted velocities and non-dimensional coefficients for the longer wavelengths were found to correspond well to linear wave theory, indicating that presence of the monopile has negligible affect on the passing flow field, as expected. For the two shorter wave periods, diffraction effects would be expected to become evident whereby the presence of the cylinder alters the wave field and the knock-on effect on the wave kinematics is apparent upstream of the cylinder.

The simulated diffracted surface elevation is also in good agreement with the analytical solutions where the presence of the cylinder has minimal effect on the surface elevation for T3 and T4; the simulated surface elevation corresponds well with the diffraction solutions for the shorter wave periods, T1 and T2. These results demonstrate that OpenFOAM can be used to approximate the diffracted surface elevation for a range of wave periods. Moreover, the use of Wang's method to determine C_d and C_m from eqns. (2) and (3) enables

values for the coefficients in eqn. (1) to be found at high β values. Calculation of the drag coefficient is notoriously difficult and solutions are limited for high β values, so comparison between the simulated values and analytical values show that viscous forces are small, which is expected for small values of *KC*.

While linear solutions provide sensible approximations for small-amplitude waves and allow direct comparison against linear diffraction solutions, future work focus on irregular waves in order to determine diffraction effects for the sea state at Teesside Offshore Wind Farm.

Acknowledgements

References

[1] G. Kieffer, T. D. Couture, Renewable Energy Target Setting, Tech. Rep., International Renewable Energy Agency (IRENA), 2015.

[2] REN21, Renewables 2016 Global Status Report, Tech. Rep., REN21 Secretariat, Paris, 2016.

[3] C. Small, R. T. Nicholls, A Global Analysis of Human Settlement in Coastal Zones, Journal of Coastal Research 19 (3) (2003) 584–599.

[4] GWEC, Offshore Wind, Tech. Rep., Global Wind Energy Council (GWEC), URL www.gwec.net/wp-content/uploads/2016/05/Global-offshore-1.pdf, 2016.

[5] I. Pineda, The European offshore wind industry - key trends and statistics 2015, Tech. Rep., European Wind Energy Association (EWEA), 2016.

[6] L. Hong, B. Moller, Feasibility study of China's offshore wind target by 2020, Energy 48 (1) (2012) 268–277.

[7] W. Krewitt, K. Nienhaus, C. Klessmann, C. Capone, E. Stricker, W. Graus, Role and potential of renewable energy and energy efficiency for global energy supply, Tech. Rep. (UBA-FB) 001323/E, Dessau-Rosslau: Federal Environment Agency (Umwelt-bundesamt), 2009.

[8] S. Capps, C. Zender, Estimated global ocean wind power potential from QuikSCAT observations, accounting for turbine characteristics and siting, Journal of Geophysical Research 115.

[9] Y. Dalgic, I. Lazkis, I. Dinwoodie, D. McMillan, M. Revie, Advanced logistics planning for offshore wind farm operation and maintenance activities, Ocean Engineering 101 (2015) 211–226.

[10] A. J. Edesess, D. Kelliher, A. G. L. Borthwick, G. Thomas, Calibrated input sea state for an offshore wind monopile in the southern North Sea, submitted for publication, 2017.

[11] V. Baagøe-Engels, J. Stentoft, Operations and maintenance issues in the offshore wind energy section: An explorative study, International Journal of Energy Sector Management 10 (2) (2016) 245–265.

[12] J. Browell, I. Dinwoodie, D. McMillan, Forecasting for Day-ahead Offshore Maintenance Scheduling under Uncertainty, in: European Safety and Reliability Conference, 2016.

[13] E. E. Halvorsen-Weare, C. Gundegjerde, I. B. Halvorsen, L. M. Hvattum, L. M. Nons, Vessel fleet analysis for maintenance operations at offshore wind farms, Energy Procedia 35 (2013) 167–176.

[14] T. Sarpkaya, M. Isaacson, Mechanics of wave forces on offshore structures, Van Nostrand Reinhold Co., 1981.

[15] M. Zdravkovich, Flow Around Circular Cylinders. Volume 1: Fundamentals, OUP Oxford, 1997.

[16] B. M. Sumer, J. Fredsøe, Advanced Series on Ocean Engineering - Hydrodynamics Around Cylinderical Structures, vol. 26, World Scientific Publishing Co. Pte. Ltd., 2006.

[17] O. M. Faltinsen, Sea Loads on Ships and Offshore Structures, Cambridge University Press, 1990.

[18] C. Y. Wang, On high frequency oscillating viscous flows, Journal of Fluid Mechanics 32 (1968) 55–68.

[19] R. C. MacCamy, R. A. Fuchs, Wave forces on piles: a diffraction theory, Tech. Rep. 69, U.S. Army Beach Erosion Board Technical Memo, 1954.

[20] R. G. Dean, R. A. Dalrymple, Water Wave Mechanics for Engineers and Scientists, vol. 2, World Scientific Publishing Co. Pte. Ltd., Covent Garden, London WC2H 9HE, 1991.

[21] N. G. Jacobsen, D. R. Fuhrman, J. Fredsoe, A wave generation toolbox for the open-source CFD library: OpenFOAM, International Journal for Numerical Methods in Fluids 70 (2011) 1073–1088.

[22] A. J. Edesess, D. Kelliher, A. G. L. Borthwick, G. Thomas, Preliminary analysis of free surface flow around a surface-piercing cylinder using OpenFOAM in the context of maintenance operations related to offshroe wind farms, accepted for publication in the 11th OpenFOAM Workshop Book, 2017.